

Large-amplitude Alfvén waves in open and closed coronal structures: A numerical study

R. Grappin and J. Léorat

Département d'Astrophysique Extragalactique et de Cosmologie, Observatoire de Meudon, France

S. Rifai Habbal¹

Department of Physics, University of Wales, Aberystwyth, Wales, UK

Received 3 August 2001; revised 26 October 2001; accepted 8 December 2001; published 16 November 2002.

[1] We present the first simulations of the coronal response to Alfvén wave injection using transparent boundaries in a classical one-fluid, isothermal axisymmetric model including both closed and open magnetic field structures. The aim of the work is first to study how Alfvén waves change the contrast between the equatorial and high-latitude wind, and second, how they modify the geometry of the wind and its global stability. We integrate the full time-dependent MHD equations, and inject large-amplitude (150 km/s), low-frequency (20 min period) waves at $1.8 R_s$, both in open and in closed field line regions, except within narrow regions around the poles and the equator. The domain considered extends up to $16 R_s$. Our principal results are the following: (1) The assumption of a latitude-independent Alfvén wave amplitude compatible with observations leads to a large acceleration both of the high-latitude and equatorial wind; as a consequence, the contrast between slow and fast wind speeds at $16 R_s$ is not as large as the observed values if extrapolated to 1 AU, a result which could potentially change with the use of better resolved, less dissipative simulations; (2) an initial delay in the Alfvén flux onset in one hemisphere generates a stable global circulation in the closed loops region, which after a long enough time produces a global north-south asymmetry and changes the structure of the corona as a whole. *INDEX TERMS:* 2149 Interplanetary Physics: MHD waves and turbulence; 2169 Interplanetary Physics: Sources of the solar wind; 7509 Solar Physics, Astrophysics, and Astronomy: Corona; 7843 Space Plasma Physics: Numerical simulation studies; *KEYWORDS:* solar wind, Alfvén waves, acceleration, nonlinear coupling, numerical simulations, MHD

Citation: Grappin, R., J. Léorat, and S. R. Habbal, Large-amplitude Alfvén waves in open and closed coronal structures: A numerical study, *J. Geophys. Res.*, 107(A11), 1380, doi:10.1029/2001JA005062, 2002.

1. Introduction

[2] During a significant portion of the solar cycle away from maximum activity, the solar wind speed at 1 AU fluctuates by about a factor two, between, say, 400 and 800 km/s, with the low values being measured close to the heliospheric current sheet where the magnetic field polarity reverses. This pole-equator contrast is already present in the acceleration region where the birth of the heliospheric current sheet is visible in white light pictures and takes the form of coronal streamers. There, the Doppler dimming method allows to draw the characteristic V structures tracing average velocity-isolines about 90 km/s [Habbal *et al.*, 1997]: these isolines envelop the streamers, suggesting that streamers are wakes in the flow around closed magnetic structures. The streamer belt could thus be viewed as a kind

of irregular magnetic grid at the inlet of the solar wind tunnel, as proposed earlier by [Mangeney *et al.*, 1991]. On the other hand, the streamer belt itself could be a source for the slow equatorial wind if the closed field regions are able to open intermittently [Wang *et al.*, 1998], while the fast wind would originate directly from the permanently, fully open regions at higher latitudes.

[3] Are we able, within the framework of isothermal MHD, to reproduce numerically the contrast between the slow and fast wind? Consider a low β , stationary axisymmetric, isothermal solution of the MHD equations within a $1/r^2$ gravitational field and an external dipolar magnetic field [Pneuman and Kopp, 1971]. Such a model is in qualitative agreement with the corona around solar minimum. Close to the solar surface, there is a stagnation zone where the plasma is imprisoned within closed magnetic loops, mimicking the irregular solar structures distributed along the equatorial belt. Above the closed loops, it shows a single equatorial current sheet where density is maximum (Figure 1 left; the quantity shown is the density compensated for radial decrease, namely $\rho r^2 \exp(1/r)$). The velocity field (Figure 1 right) shows the same symmetry: the flow is

¹Also at Harvard-Smithsonian Center for Astrophysics, Cambridge, Massachusetts, USA.

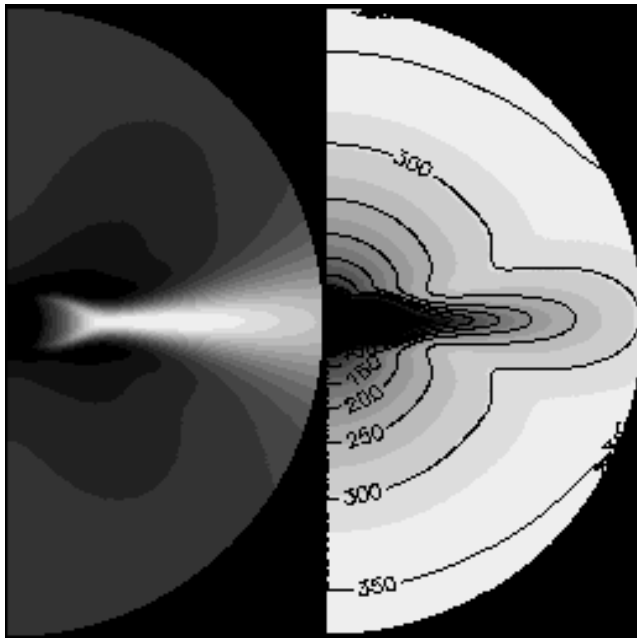


Figure 1. Stationary MHD solution between 1.8 and 16 R_s . Axisymmetric, isothermal wind within an external magnetic dipole ($\beta = 0.017$ at poles, 0.086 at equator). Left: density compensated for radial decrease. Right: radial velocity.

slower within the equatorial current sheet than at larger latitudes.

[4] However, when comparing the velocity profiles of this solution at polar and equatorial latitudes (Figure 2), one sees that the high contrast which holds at 5 R_s rapidly fades away with distance, the polar wind becoming only 20% faster than the equatorial wind at 16 R_s ; when extrapolated up to 1 AU, this is much lower than the real contrast (i.e., the factor of two mentioned above), and the velocity gradient is substantially lower than the fast wind speed measurements at 2 and 3 R_s [Esser *et al.*, 1999] (hatched, bold lines in Figure 2). Hence clearly the model wind at the pole is already lacking momentum at this distance.

[5] In summary, in a stationary isothermal MHD solution, the polar wind is too slow, and the flow tends to become spherically symmetric as distance increases. In principle, Alfvén waves can provide some of the missing momentum [Alazraki and Couturier, 1971]. However, does this momentum decrease or increase the contrast between polar and equatorial wind? We do not know the answer, because no global study of the nonstationary wind driven by Alfvén waves has ever been published. Nonstationary models either deal with purely open regions, as in the work of Lau and Siregar [1996] and Ofman and Davila [1998], or, as in the work of Usmanov *et al.* [2000], use a wave pressure model in which only the linear propagation of the Alfvén waves is taken into account, and the wave amplitude is arbitrarily reduced in the whole closed region.

[6] Our aim is to study the full dynamical interaction of waves and ambient wind, by introducing them into both closed and open regions. We remain here within the classical framework of isothermal, axisymmetric MHD; specifically, we begin wave injection starting from the

configuration represented in Figure 1. If Alfvén waves with large enough amplitudes to accelerate the wind are indeed present, they must do more than just accelerate the wind. Alfvén waves may well modify the closed field structure itself which in turn could modify the flow in open regions. In this case, do the closed regions remain just a barrier, or are they a source of mass flux themselves, as in the model of Einaudi *et al.* [1999] where a shear flow imbedded in a neutral sheet leads to intermittent mass ejections when the appropriate unstable modes are excited? The north-south symmetry comes out naturally when dealing with an external dipole field (see Figure 1). How stable is this configuration in the presence of Alfvén waves which are large enough to yield a fast wind?

2. Numerical Approach

[7] To address the above mentioned problem, we use transparent boundaries, as in Grappin *et al.* [2000] where propagation of small-amplitude Alfvén waves was studied. By transparent boundaries, we mean that fluctuations propagate through the boundaries as if there was no boundary at all (without reflections). On the other hand, fluctuations propagating into the numerical domain from outside are prescribed, or more precisely their evolution equation at the boundary is prescribed. Such conditions are appropriate for the distance range considered, well above the solar surface. This choice of transparent boundaries is at odds with most studies in which the normal velocity at the inner boundary is either set to zero (in studies of the coronal heating by waves as Belien *et al.* [1999], or allowed to assume only positive values [Usmanov *et al.*, 2000]. In fact, only transparent boundaries allow the plasma to circulate downward (toward Sun) as well as upward (away from Sun), and this has, as we shall see, important consequences on the dynamics of the corona and solar wind as a whole.

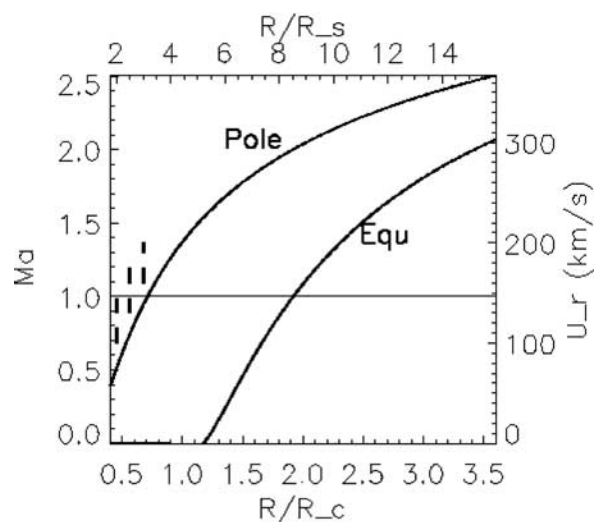


Figure 2. Stationary MHD solution as in Figure 1: polar and equatorial radial cuts. Left and bottom axis give the Mach number versus distance normalized to the sonic radius. The right and top axis give the velocity in kilometers per second (assuming a coronal temperature of 1.3×10^6 K) versus distance in solar radii. Bold, hatched lines indicate solar wind speed estimations by Esser *et al.* [1999].

[8] Injecting waves via transparent boundaries requires some care in the choice of spatial schemes, in order to prevent the onset of instabilities at the inner boundary [see *Grappin et al.*, 2000]. Here, passing from small to large-amplitude Alfvén waves, and from medium to low β has necessitated to modify in part the dissipation scheme compared to that reported by these authors. In particular, filtering was replaced by diffusive (Laplacian) terms at the boundary for the magnetic potential on the one hand, and everywhere for the velocity, except within ten mesh points from the inner boundary (between 1.8 and 2.3 R_s), where only the transverse contribution of the Laplacian was kept.

[9] What are the control parameters in this problem? The origin of the momentum transfer from waves to the bulk plasma flow lies in the vertical gradient of the magnetic wave pressure which should decrease with height, both due to stratification and dissipation. While the amplitude of the incoming waves must be fixed, the characteristic decay length of the wave is not a free parameter here, at variance with models based on wave pressure terms [*Jacques*, 1977; *Usmanov et al.*, 2000]. Instead, here, the wave damping is the consequence of nonlinear steepening and wavefront deformation due to Alfvén speed gradients (phase mixing), two processes which in part depend on the numerical setup (resolution in particular), but basically are determined by physical processes and so should not be independently fixed.

[10] The numerical domain is a spherical shell between 1.8 and 16 R_s . The temperature of the corona is assumed to be 1.3×10^6 K. A monochromatic wave of about 150 km/s in rms amplitude is injected at 1.8 R_s , which is comparable to observed upper bounds [*Essex et al.*, 1999]. The wave period is monochromatic, with period equal to 20 min. This choice is not critical, only convenient. One may note that this period falls within the Alfvénic range observed in situ at larger distances. Also, the resulting wavelength contains a substantial number of grid points, which ensures that the wave is not immediately damped. In a given hemisphere, the phase of the wave does not depend on latitude. However, in order to depart from too perfect a symmetry between the Northern and Southern Hemispheres, one introduces a delay between the injection onset in each; the Northern Hemisphere is perturbed first, then the southern hemisphere 50 min later. As we will see, the resulting (long term) asymmetry is not directly related to this initial asymmetry.

[11] The latitudinal extent of the Alfvén wave perturbation is limited in two ways. First, the poles must remain unperturbed, because, due to axisymmetry, no transverse perturbation can be injected there. Second, injecting Alfvén waves right at the equator would induce a gradient (shear) either in the transverse components of the velocity, and/or of the magnetic field, which would scale as the inverse of the mesh size [see *Grappin et al.*, 2000]. We prefer here not to include such a shear which could be suspected to be unphysical. Note that although the absence of polar perturbation clearly forbids any comparison with the observed polar wind, the properties of the (fast wind) midlatitude region between 20 and 55 deg from equator will prove to be almost latitude-independent, so that one can be reasonably confident that the absence of polar perturbation does not affect strongly the middle- and low-latitude regions.

[12] We report here on two numerical experiments which differ by the extent of the unperturbed zone around the

equator. In both runs, the unperturbed zone around the pole lies within 7 deg from poles. In run 1, the unperturbed zone around the equator lies between -12 and 12 deg. In run 2, the unperturbed zone lies between -5 and 5 deg. There is no other difference between the two runs.

3. Results

[13] Figure 3 allows to compare the amplitude and latitude extent of the perturbation with that of the unperturbed flow. It shows some profiles (density, radial component of magnetic field, and velocity) of the stationary flow at the inner boundary, together with several profiles of the azimuthal velocity, sampled regularly during the first period of the wave injection for run 2, that is, for the run with the narrowest still zone around the equator. Several important characteristics of the experiment are visible in the figure. First, only the northern hemisphere is excited at that time, since, as mentioned above, the excitation starts in the other hemisphere 50 min later. Nevertheless, a small bump becomes visible in the Southern Hemisphere. This bump is the signature of downward propagating waves from the other hemisphere along the closed loops. The small gap between the main northern plateau and the bump in the south traces the unexcited region around the equator for this run 2. Finally, the narrowness of the bump (compared to the large extent of the closed loops region) is related in part to the larger propagation times along long loops, but also, as we shall see, to the higher level of dissipation along the longest loops.

[14] Figure 4 uses the same presentation as Figure 1 to show the state of the wind after 33.5 hours of wave injection (note however that it is not the instantaneous radial velocity that is shown, but its time average during one Alfvén period, which is much clearer). At that time, the wind has reached a quasi-stationary regime, i.e., both the slow and fast winds have travelled the whole distance domain. The comparison with Figure 1 shows that the slow equatorial region has become narrower. The equatorial wind has now a substantially higher speed than previously without waves. Outside the equatorial current sheet, one must distinguish the polar region, which is slow because there is no wave injection (actually substantially slower than without waves, due to global reorganization of the wind geometry), and a fast wind midlatitude region which extends from about 20° to 55° from equator, in a large portion of the domain.

[15] The density proves to be systematically smaller in the perturbed flow; the density drop is maximal in the excited regions closest to the equatorial current sheet. The poloidal velocity is substantially larger than in the time-independent flow. This corresponds to a stronger focussing of the midlatitude flow towards the ecliptic in the presence of waves; the flow in both cases becomes radial when the distance increases, but the trend is slower in the presence of waves.

[16] Figure 5 allows a detailed comparison between the midlatitude (45°) and equatorial regions, both for the unperturbed and perturbed wind. One shows radial cuts of the radial and azimuthal velocities at the equator and at 45° latitude. Thick lines show the (instantaneous) perturbed wind profiles, and plain lines the unperturbed wind. A striking feature of the perturbed wind is that both the

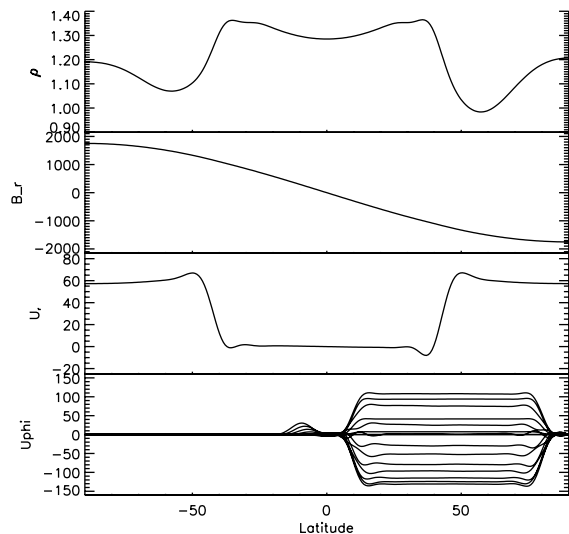


Figure 3. (Run 2) Inner boundary profiles: onset of perturbation and stationary MHD solution. From top to bottom: density, radial component of magnetic field, and velocity for the stationary MHD solution (Figures 1 and 2); bottom: azimuthal component of the velocity sampled during the first period of wave injection (recall that the Northern Hemisphere is perturbed first). Units for U_r and U_ϕ : kilometers per second; units for density ρ and B_r are arbitrary.

midlatitudes and the equator show large speed increase. Indeed, in spite of the almost complete damping of the Alfvén wave flux (bottom figure), the equatorial wind reaches 400 km/s at the outlet, to be compared with the

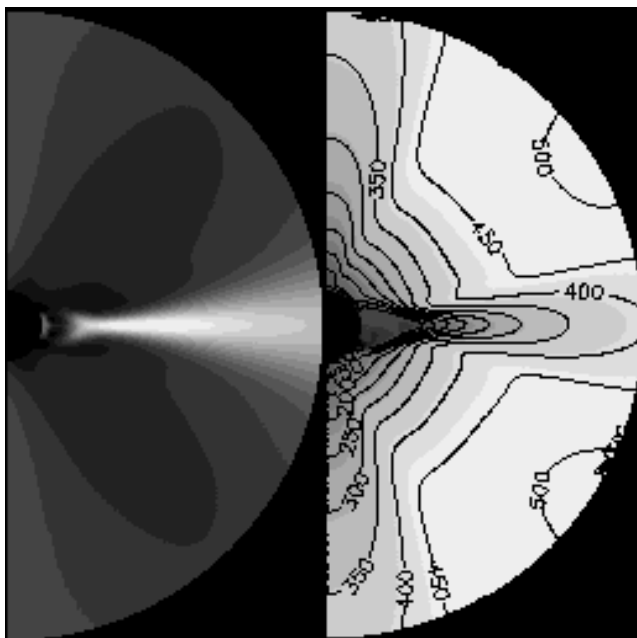


Figure 4. (Run 1) MHD wind accelerated by Alfvén waves, after 33.5 hours injection. Left picture: density compensated for radial decrease. Right picture: radial velocity, averaged during one Alfvén period. The slow velocity at the poles is a direct consequence of the absence of Alfvén wave injection there.

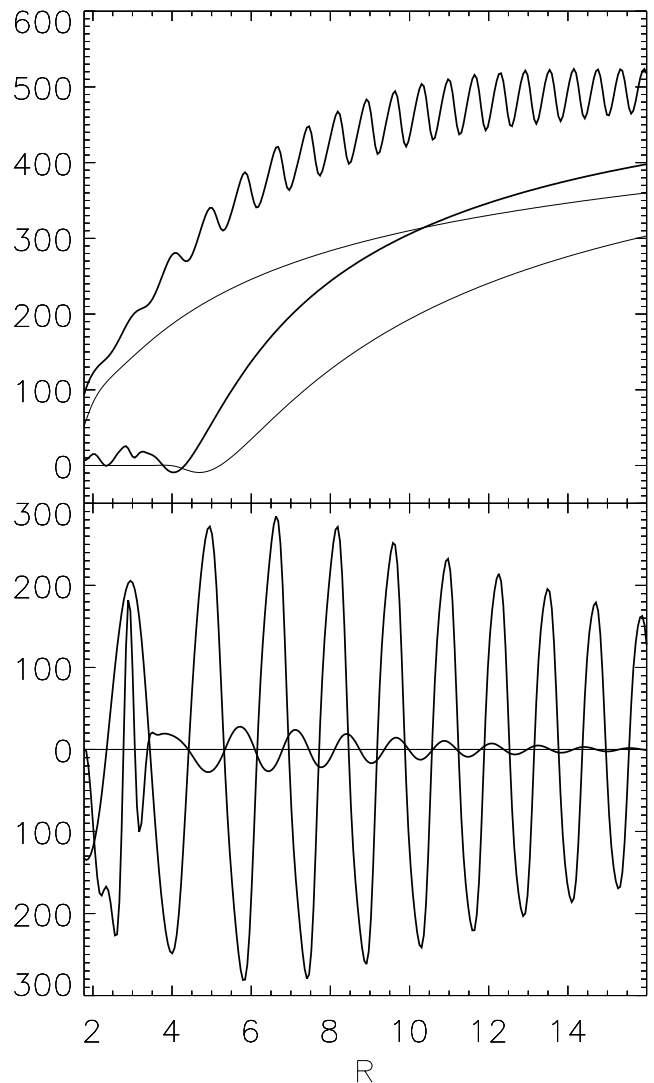


Figure 5. (Run 1) Comparison between the wind accelerated by Alfvén waves after 33.5 hours injection (bold lines) and the stationary wind (plain lines). Radial profiles at equator and 45° latitude: radial velocity (top) and azimuthal velocity (bottom).

former value of 300 km/s without waves. As a consequence, the contrast at the outlet between the maximum (high-latitude) wind velocity and the minimum (equatorial) wind velocity is not much enhanced: from 1.2 in the stationary flow, it becomes 1.4 for the perturbed flow. Moreover, this contrast is seen to decrease with distance so that extrapolating from 16 R_s to 1 AU clearly cannot meet the observed factor of two. We will come back on this point in the discussion.

[17] The pattern of the azimuthal velocity in Figure 5 (bottom) departs from the monochromatic pattern one would expect from monochromatic excitation: this results from the nonlinear steepening. The distance range can be subdivided into two intervals: in the first interval, the radial profile follows closely the WKB prediction, while in the second, damping (associated with nonlinear steepening or phase mixing due to transverse gradients of the Alfvén speed) is important. The reader is referred to the paper by

Grappin *et al.* [2000], which shows the same kind of phenomena, in the case of smaller amplitude waves. Note that this does not necessarily contradict the observations by Roberts *et al.* [1990] that the wave amplitude follows on average the WKB decrease, since the latter observations deal with larger heliocentric distances where, the wave amplitude being smaller, the steepening and subsequent dissipation and transfer should proceed at a smaller rate.

[18] To summarize, the Alfvén wave amplitude reaches a maximum of about 300 km/s around $6 R_s$, with rms values about 100 to 150 km/s at the inner boundary. As a consequence, the density contrast between the current sheet and the surrounding plasma is enhanced. Most importantly, the high-latitude velocity becomes comparable at $3 R_s$ with observed values [Esser *et al.*, 1999], but the equatorial radial velocity is also much enhanced, in spite of the fact that the Alfvén waves are completely absent from the equator. As a consequence, the polar/equatorial contrast remains clearly insufficient, when extrapolated, to match values observed at 1 AU. These features are valid for run 1 as well as run 2.

[19] The flow configuration just described is actually not stationary, and shows a complete reorganization during the next day of perturbation, different for runs 1 and 2. Figure 6 gives a global picture of the evolution: one shows eight density snapshots (compensated for radial decrease) for run 1, spaced every 8.4 hours, starting with the unperturbed flow. The figure is to be read from left to right and top to bottom. The flow regime shown in Figure 4 corresponds to the picture bottom left.

[20] The successive steps are as follows. First (pictures 2 and 3, top) the latitude span of the current sheet increases, because of a snowplow effect: a cut along a magnetic field line indicates that, during this first phase, the radial velocity profile has a peak which propagates outward from the Sun, so that matter accumulates ahead of this peak. A quasi-equilibrium flow establishes within around 24 hours, in which the dense current sheet appears thinner than initially in the stationary flow, where very low density lanes on the boundaries of the dense current sheet are visible (compare pictures 1 and 4 in Figure 6). This is due to the dynamic ram pressure of the fast streams focussing strongly towards the equator, and thus pushing the current sheet, as discussed above.

[21] During the following phase, a progressive destabilization of the whole configuration takes place, leading to a flow (last picture), in which the current sheet has lost the north-south symmetry. Although this is not conspicuous since later times are not shown, this last flow configuration does not evolve subsequently.

[22] This final stationary flow is not the only asymptotic state possible. One might think that it reflects essentially the initial asymmetry, i.e., the fact that we inject first waves in the Northern Hemisphere. This is not so. Indeed, if we still inject waves first in the northern hemisphere, but change the latitude interval in which Alfvén waves are injected, as in run 2, one obtains an asymptotic flow which is quite similar to that of the last picture in Figure 6, but with the opposite north-south asymmetry (see Figure 7), which shows the velocity contours for runs 1 and 2 at the final stage).

[23] The origin of the global loss of symmetry lies in a systematic circulation which takes place first in the shortest

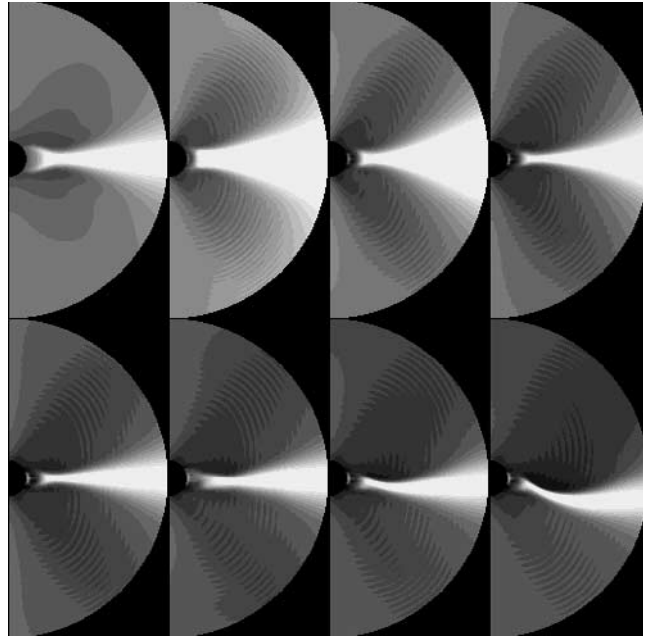


Figure 6. (Run 1) Long-term evolution induced by Alfvén waves, starting with the stationary solution. Density compensated for radial decrease. Time lapse between two successive pictures: 8.4 hours.

closed loops. To show this circulation and how it extends to higher distances, we show in Figure 8 a close-up of the equatorial region, comparing the flow configuration for both runs 1 and 2 after 33.5 hours (at the time of the fast symmetric flow), and after 58.7 hours (when the global current sheet has reached its final asymmetric equilibrium state). Note that the figure gives the flow velocity and the isocontours of Alfvén velocity, showing the correlation between both, at least in the early stage.

[24] Consider first the symmetric stage (left of Figure 8). In both runs, we see a large central region devoid of Alfvén fluctuations (shown are isocontours of u_ϕ). This is due to the very large dissipation associated with the shear of wavefronts (phase mixing) by strong Alfvén speed gradients. In the region where Alfvén waves are present (because they are injected, and undamped), one observes a circulation, which is in opposite directions for runs 1 and 2, and actually much stronger for run 2. This circulation has no appreciable consequence at that time on the distant wind, which still shows the north-south symmetry.

[25] After 58.7 hours, the initial circulation has spread among much longer loops, at larger distances. This has led to a strong ram pressure of the circulating flow coming from one hemisphere onto the current sheet, which is thus being pushed away from the equator, leading to a very thin current sheet away from the equator as seen previously in Figures 6 and 7.

4. Discussion

[26] We have injected monochromatic quasi-planar Alfvén waves at almost all latitudes within the inner boundary ($1.8 R_s$) of an isothermal, axisymmetric corona with a low β . The wind gains additional momentum from

the waves at almost all latitudes (except within a cone around the poles where no waves are injected). The speed gain is substantial also at the equator, although the Alfvén waves show but a small amplitude when reaching the heliospheric current sheet. As a result, the contrast between the slow wind close to the heliospheric current sheet and the higher latitudes is enhanced compared to the stationary wind with no waves, but is still too small when compared to the observed solar wind. Note that the simulations with wave pressure modeling by [Usmanov *et al.*, 2000] show a contrast much more compatible with solar wind data. Two factors probably contribute to this difference: first, the dissipation is reduced compared to ours, since these authors use an exponential radial grid in the strongly stratified region, while we use a uniform grid; second, they have no Alfvén flux in the equatorial region. A visible effect of the diffusion in our simulations is for instance the increase of the angular size of the heliospheric current sheet with distance. Runs using a larger resolution and thus reduced dissipation are planned to investigate this issue.

[27] It might also be that compressive waves are more important close to the current sheet, which would eventually lead to a slower low-latitude wind, as suggested by an analysis of acoustic perturbations of nonmagnetic winds [Grappin *et al.*, 1997]. In the future, we plan to investigate

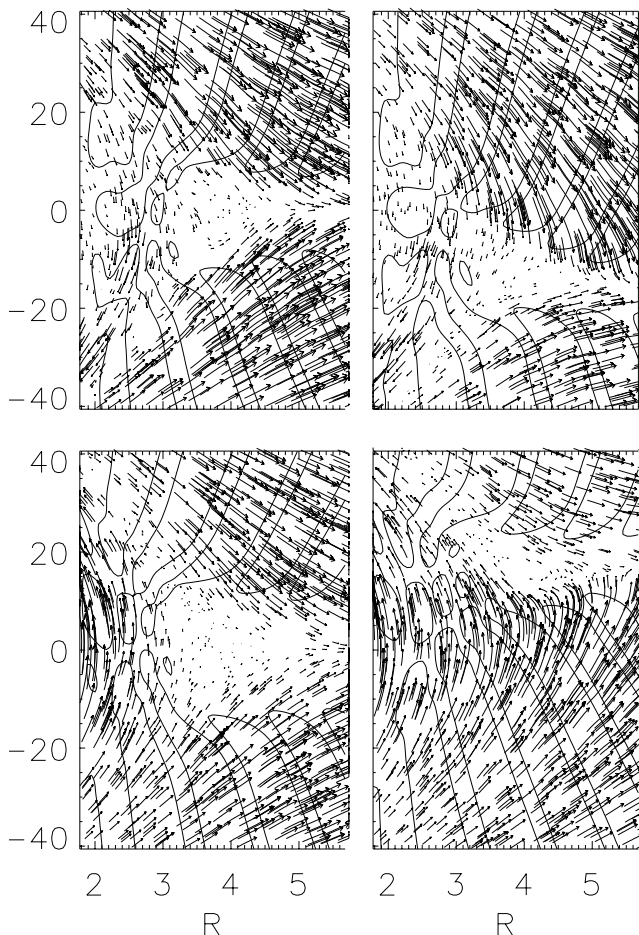


Figure 7. Radial velocity structure of the flow in runs 1 (left) and 2 (right), after 58.7 hours of Alfvén wave injection.

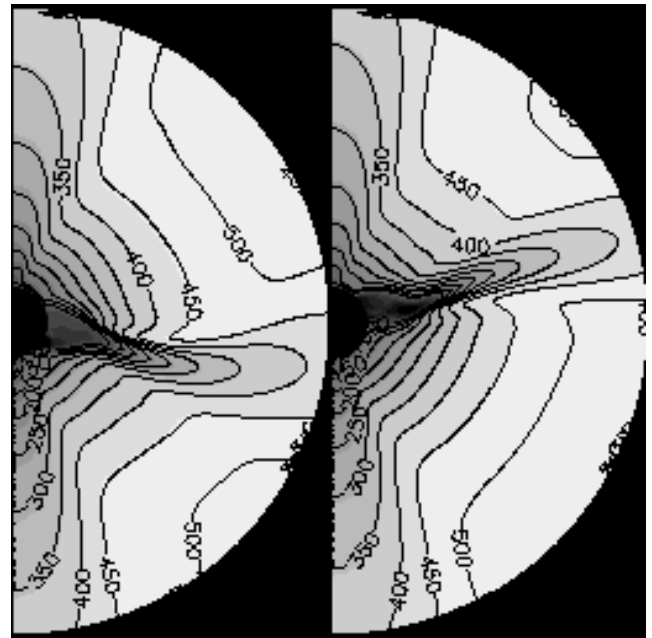


Figure 8. Close up of the closed field region: circulation along closed loops. Top: run 1. Bottom: run 2. Left: after 33.5 hours injection. Right: after 58.7 hours injection. Isocontours for $u_\phi = -100$ km/s and 100 km/s.

the response of the corona to compressive waves to answer this point.

[28] The main new result reported here is the possibility that Alfvén waves destabilize the corona and solar wind, starting with a global circulation in the closed loops region. This was not observed in previous simulations, due to too restrictive boundary conditions. The phenomenon can probably be obtained in various ways, the necessary condition being that the velocity at the inner boundary in the closed field region must not be fixed to zero, but instead left free to vary.

[29] What determines the onset of the circulation? Figure 9 shows the various quantities characterizing the circulation at the inner boundary, for runs 1 (top) and 2 (bottom). One sees that, while the upward wave component is approximately constant in the expected range, the downward wave amplitude is substantial only in a restricted latitude range, and that its amplitude is different in both hemispheres. Also, the density level at the corresponding latitudes is varying. Note that the correlation between density and downward amplitude, the upward amplitude being fixed, is expected if one assumes that the WKB invariant is at least partly valid. These north-south asymmetries are correlated for all quantities, that is, they correspond to a definite direction of circulation, north to south or reverse, as seen in the right panels. To be specific, the condition for the onset of the circulation seems to be an imbalance between the global wave amplitude gradient between both hemispheres. The extreme speed of the circulation (700 km/s) observed in the case of run 2 (localized close to the inner boundary, as seen in Figure 8), is probably a consequence of the specific conditions of the run. It is likely, for instance, that introducing some randomness in the wave injection would lead to a slower, more reasonable circulation speed.

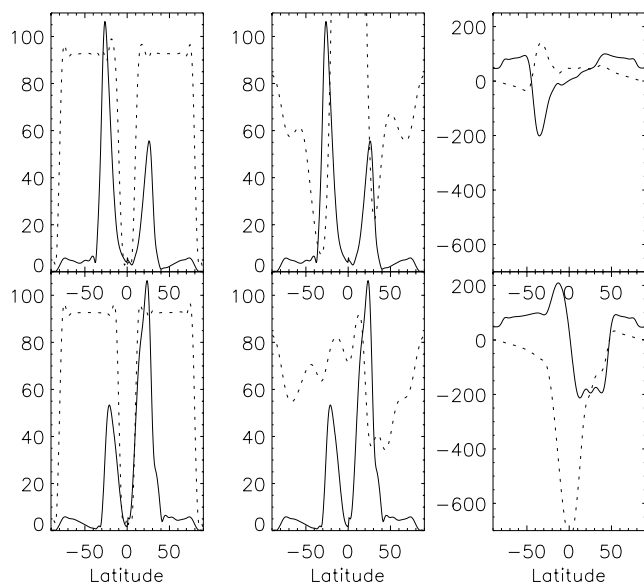


Figure 9. Inner boundary, rms, and average quantities (computed during one wave period) in the final stationary regime. Runs 1 (top) and 2 (bottom). Left: rms downward propagating wave amplitude (solid), rms upward propagating wave amplitude (dotted); Middle: rms downward propagating wave amplitude (solid), average density (dotted); right: average radial velocity (solid), poloidal velocity u_θ (dotted). Units: kilometers per second, except for density unit which is arbitrary.

[30] In the present simulations, the amplitude of upward propagating waves being fixed and identical in both hemispheres, the wave pressure imbalance is due to a substantial variation of the density between footpoints in both hemispheres, which in turn induces variations in the amplitude of downward propagating waves (as seen for instance when considering the WKB invariant).

[31] The constraint of fixing the amplitude of upward propagating waves at $1.8 R_s$ seems however not completely satisfactory. In a real atmosphere, the amplitude of upward propagating waves at a given height is indeed likely to vary with the density, as well as the downward amplitude, so leading probably to no net imbalance in the magnetic wave pressures from north and south footpoints of a given loop. This does not mean that the same kind of circulation cannot occur on the Sun, but only that it is probably driven more directly by differences in the upward Alfvén flux injected at the two magnetic footpoints of a given loop at the solar surface.

[32] Further investigations are needed in order to elucidate both the conditions for destabilization and the mechanism for the spreading of the circulation, i.e., its transformation into a global asymmetric flow.

[33] How relevant are such large deviations from the north-south symmetry? The real Sun deviates largely both from perfect north-south symmetry, and from axisymmetry as well, even at solar minimum; this non-axisymmetry should make more complex the final configurations discussed here. What would be the result of a simulation which would relax the axisymmetry constraint, keeping the exter-

nal dipole? It is probable that we would obtain not one, but very many (an infinity?) of quasi-equilibrium configurations, which might be all unstable in three dimensions, thus providing for random and chaotic fluctuations. However, it might also be that, keeping the axisymmetric constraint, but with lower dissipation (higher resolution), the asymmetric configurations are no longer stable, in which case the heliospheric current sheet would oscillate and become a turbulent region (and not laminar as in this work), but still devoid of clear signature for Alfvénic fluctuations, which would agree well with in situ observations. Such fluctuations would provide the seed for the solenoidal part of the lowest frequencies (non-Alfvén component) of the turbulent spectrum observed in situ at larger distances. This would not be contradictory to the intermittent emission of dense blobs, which would be triggered not by Alfvén waves, but by other wave modes, to be studied in a later work.

[34] **Acknowledgments.** We thank IDRIS for providing numerical facilities (project 010219). Michel Blanc thanks Arcadi V. Usmanov and Melvyn L. Goldstein for their assistance in evaluating this paper.

References

- Alazraki, G., and P. Couturier, Solar wind acceleration caused by the gradient of Alfvén wave pressure, *Astron. Astrophys.*, *13*, 380–389, 1971.
- Belien, A. J. C., P. C. H. Martens, and R. Keppens, Coronal heating by resonant absorption: The effects of chromospheric couplings, *Astrophys. J.*, *526*, 478–493, 1999.
- Einaudi, J. G., J. P. Boncinelli, J. B. Dahlburg, and J. J. Karpen, Formation of the slow solar wind in a coronal streamer, *J. Geophys. Res.*, *104*, 521–534, 1999.
- Esser, R., S. Fineschi, D. Dobrzycka, S. R. Habbal, R. J. Edgar, J. C. Raymond, and K. L. Kohl, Plasma properties in coronal holes derived from measurements of minor ion spectral lines and polarized white light intensity, *Astrophys. J.*, *510*, L63–L67, 1999.
- Grappin, R., E. Cavillier, and M. Velli, Acoustic waves in isothermal winds in the vicinity of the sonic point, *Astron. Astrophys.*, *322*, 659–670, 1997.
- Grappin, R., J. Léorat, and A. Buttighoffer, Alfvén wave propagation in the high solar corona, *Astron. Astrophys.*, *362*, 342–358, 2000.
- Habbal, S. R., R. Woo, S. Fineschi, R. O’Neal, J. Kohl, G. Noci, and C. Korendyke, Origins of the slow and ubiquitous fast solar wind, *Astrophys. J.*, *489*, L103–L106, 1997.
- Jacques, S. A., Momentum and energy transport by waves in the solar atmosphere and solar wind, *Astrophys. J.*, *215*, 942–951, 1977.
- Lau, Y.-T., and E. Siregar, Non-linear Alfvén wave propagation in the solar wind, *Astrophys. J.*, *465*, 451–461, 1996.
- Mangeny, A., R. Grappin, and M. Velli, MHD turbulence in the solar wind, in *Advances in Solar System Magnetohydrodynamics*, edited by E. R. Priest and A. W. Hood, pp. 326–356, Cambridge Univ. Press, New York, 1991.
- Ofman, L., and J. M. Davila, Solar wind acceleration by large-amplitude nonlinear waves: Parametric study, *J. Geophys. Res.*, *103*, 23,677–23,690, 1998.
- Pneuman, G. W., and R. A. Kopp, Gas-magnetic field interactions in the solar corona, *Sol. Phys.*, *18*, 258–270, 1971.
- Roberts, D. A., M. L. Goldstein, and L. W. Klein, The amplitudes of interplanetary fluctuations: Stream structure, heliocentric distance, and frequency dependence, *J. Geophys. Res.*, *95*, 4203–4216, 1990.
- Usmanov, A. V., M. L. Goldstein, B. P. Besser, and J. M. Fritzer, A global MHD solar wind model with WKB Alfvén waves: Comparison with Ulysses data, *J. Geophys. Res.*, *105*, 12,675–12,695, 2000.
- Wang, Y. M., N. R. Sheeley Jr., J. H. Walters, G. E. Brueckner, R. A. Howard, D. J. Michels, P. L. Lamy, R. Schwenn, and G. M. Simnett, Origin of the streamer material in the outer corona, *Astrophys. J.*, *498*, L165–L168, 1998.

R. Grappin and J. Léorat, Département d’Astrophysique Extragalactique et de Cosmologie, Observatoire de Meudon, 92195 Meudon, France.
S. R. Habbal, Department of Physics, University of Wales, Aberystwyth, Ceredigion SY23 3BZ Wales, UK.